Materials Research. 2017; 20(Suppl. 2): 273-278
DOI: http://dx.doi.org/10.1590/1980-5373-MR-2017-0083

Effects of Solidification Rate in the Microstructure of Al-Si5Cu3 Aluminum Cast Alloy

Maria Eduarda Farina[a]*, Pedro Bell[a], Carlos Raimundo Frick Ferreira[b], Berenice Anina Dedavid[a]

[a]Engineering Faculty, Pontifical Catholic University of Rio Grande do Sul (PUCRS), Porto Alegre, RS, Brazil
[b]Foundry Laboratory, Department of Metallurgy, Federal University of Rio Grande do Sul (UFRGS), Porto Alegre, RS, Brazil

Received: January 17, 2017; Revised: May 10, 2017; Accepted: June 20, 2017

Aluminium alloy Al-Si5Cu3 (319) is one of the most commonly used casting alloys for automobile components, due to its casting characteristics. Iron is the major impurity element that influences the detrimental β-phase formation in secondary aluminum alloys. In the present study, we investigated the influence of the cooling rate on the formation of iron compounds, α-$Al_{15}(Mn,Fe)_3Si_2$ and β-Fe_5AlSi phases, in Al-Si5Cu3 containing 1.0% Fe, 0.5% Mn and 0.2% Mg, by thermal analysis and metallography. The results show that the high cooling rates, between 10-10^3 K/s, are able to reduce and nullify the formation of needle-like β-Al5FeSi phase, and help the formation of the Chinese scripts α-$Al_{15}(Fe,Mn)_3Si_2$ phase. The analysis of the curves reveals that the increase of the cooling rate increases the temperature of nucleation of the α-Al dendrite and decrease the eutectics Al-Si and Al-Cu phases.

Keywords: *Solidification, Al-Si alloys, iron-compounds, thermal analysis, CA-CCTA*

1. Introduction

The casting process is more economical than any other process of metal manufacture, provided that the melting point is lower than 1800ºC[1]. Although the manufacturing path from the liquid to the finished shape is the most direct, this involves a simultaneous control of the processes parts, including melting, alloying, molding, pouring, solidification process and finishing. Therefore, it is not surprising that the production of castings is a challenging technology[1,2].

The main aluminum alloys castings contain silicon due to its capability to increase fluidity, elevated temperature resistance to cracking, and feeding characteristics[1,2]. In addition, silicon is the only alloying element that added to aluminum does not increase the specific mass of the alloy. Copper and magnesium increase strength and toughness in Al-Si alloys, as well as provide hardening phases that precipitate during the aging thermal treatment[1,2]. The major impurity element in Al-Si alloys that influences the detrimental secondary phase formation is iron, usually acquired during the recycling process[2,3].

Unfortunately, there is no economically viable way known to remove the iron of aluminum alloys. Consequently, the iron compounds continue to increase potentially with every remelting cycle in foundry activities[1,2,5].

The commercial AA 319 (Al-Si5Cu3) cast alloy has excellent mechanical properties, which makes it suitable for use in many automotive applications. However, using recycled-grade Al-Si and Al-Cu alloys as the base material for structural components remains a major challenge, especially when fatigue life is critical[2-6,8,11-13].

During a conventional solidification of the Al-Si5Cu3 alloy, the first reaction is the nucleation and growth of the α-Al dendrite. Thus, the pro-eutectic Fe-containing phases take place. The Al-Si eutectic phase, the Mg_2Si and the Al_2Cu precipitation occur successively[6].

The iron-containing compounds that form during solidification processes appear in a few shapes and sizes, usually divided into three different morphologies: β-Fe_5AlSi needles, α-$Al_{15}(Mn,Fe)_3Si_2$ Chinese script (also called α_c-phase) and polyhedral crystals[5,6]. The β-Fe_5AlSi intermetallic compound is hard and brittle, having low cohesion with the aluminum matrix. It acts as crack initiators and plays a role in forming solidification defects, such as porosity and hot tearing, being detrimental to in-service mechanical properties of the cast components cast[4-8].

Several researchers[2-6,8,11] observed that the damaging effects of iron can be minimized through some techniques, such as the rapid-solidification process, iron/manganese ratio control and the superheat melting before pouring. These methods basically convert the crystallization of the needle-like β-Fe_5AlSi phase into the less damaging α_c-$Al_{15}(Mn,Fe)_3Si_2$ phase[6-8-10,11,13].

This subject is not yet completely exhausted considering that solidification of commercial alloys is complex and behaves far from the equilibrium conditions[1]. In the design of cast components, it is necessary to monitor the solidification of alloys under different cooling conditions corresponding to different cross sections of the castings[1,2,8-11].

In the present work, we studied the microstructural behavior of iron containing intermetallic compounds in the 319.2 aluminum alloy as a function of cooling rate, through

* e-mail: maria.tedesco@acad.pucrs.br

computer-aided cooling curve thermal analysis (CA-CCTA) and metallography.

The CA-CCTA is a quantitative and non-destructive on-line process control method used in different processes in aluminum cast alloys[9,12]. This thermal analysis method is based on the cooling curves (temperature x time) obtained during the solidification of the alloy from the liquid phase. The cooling curve reflects the release of latent heat during the metal cooling in the solidification. Differently from other techniques, such as the Differential Thermal Analysis (DTA) and the Differential Scanning Calorimetry (DSC), CA-CCTA do not dependent on a sample size, nor on continuum rates of heating and cooling. CA-CCTA method is simple, inexpensive, provides consistent results and, consequently, the most suitable for foundry applications[12].

The cooling rates used in this work are similar to those found in foundry industrial processes[2]. Cooling rates in the semi-solid region of about 10^{-1} to 10^{3} K / s were acquired with the use of a tec-tip standard cup and a six-stepped cylindrical steel mold[1,2].

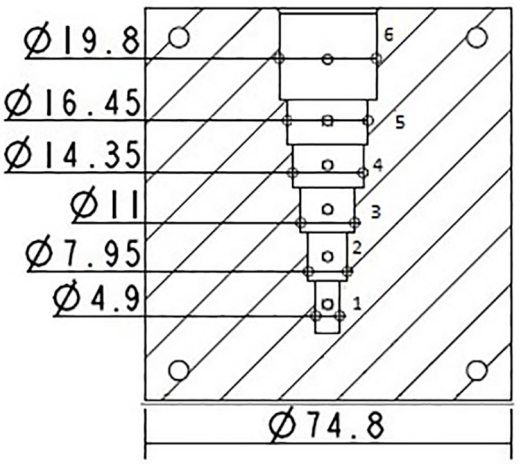

Figure 1. Schematic of six-stepped cylindrical steel mold used in the present work.

2. Experimental Procedure

In this study, the Al-5Si3Cu alloy was prepared and melted with commercial base Al-9% Si, Al-Cu and aluminum ingots, followed by the addition of iron and manganese in powder form. The chemical compositions of all ingots studied were verified by optical emission spectrometry using the SPECTROMAXx stationary metal analyzer by SPECTRO®, as shown in table 1. In the present study, neither grain refiner nor eutectic modifier were added to the melt.

We carried out the casting process with about 500 g of alloy melt in an electric-resistance furnace, in a commercial graphite crucible, held at a temperature of around 993 K. Before pouring, the melts were skimmed and held for 20 min at approximately 1123 K. A high temperature of pouring (1073 K, i.e. ~ 200 K above of *liquidus* point) was used so that the acquisition system was able to record the data above the *liquidus* point.

To obtain several solidification conditions, we used tec-tip standard cups and a cylindrical metallic stepped-mold having six sections with different diameters (see figure 1). A metallic pouring-cup was adapted to the step-mold to drive the melt to flow down.

In the metallic six-stepped mold, temperature x time data for thermal analysis was conducted by five thermocouples type K (Ni-Cr-Ni) high sensitive, with 0.508 mm of diameter, and protected in a stainless steel sheath. To increase the sensitivity of system response, the tips of the thermocouples were stripped. The data were acquired by modular National Instruments system (A/D converter) with response time of 10^{4} Hz, through lab view 5.0 software. Parameters such as cooling rate, initial and final solidification time as well as the temperature and time of nucleation of the phases were identified for each mold.

The microstructural examination and Vickers microhardness measurements were realized in samples cut transversely of ingots obtained in the tec-tip standard cup and metallic stepped-mold. In order to correlate the thermal analysis parameters with the alloy microstructure, the observations of samples were realized in the region near the tips of the thermocouples. The samples were prepared by the conventional metallographic method and etched by HF solution (1ml of HF for 200ml of H_2O)[1,2]. The microstructure analysis was carried out through Olympus BH2 optical microscopy, Scanning Electron Microscopy FEG Inspect F50 – FEI®, and microanalysis by Energy Dispersive Spectroscopy (EDS) with an OXFORD® AZtecOne^{XT} system detector. The average size of α-Al grains were measured by the linear intercept method according to the ASTM-E112-96[14]. In order to compare the hardness to the solidification rate, per ASTM E384[15], we carried out Vickers microhardness measurements using the Shimadzu® HMV-G.

Table 1. Chemical Composition of 319 (Al-5Si3Cu) aluminum alloy (wt %). (*) Ref. 2.

Alloy	Type	Si	Cu	Fe	Mn	Mg	Zn	Ti	others	Al
319.1*	Limits	5.0-6.0	4.0-5.0	1.0	0.5	0.1	1.0	0.25	0.5	bal
319.1*	Nominal	6.0	3.50	...	...	...	...	...	...	...
319.2	Ingots studied	5.54	3.06	1.0	0.5	0.2	0.96	0.01	0.2	bal

3. Results and Discussion

3.1. Solidification in low cooling rate

In figure 2, it is possible to observe the cooling curve (Temperature (K) / time (s)), the first derivative and second derivative curves (dT/dt and d^2T/dt^2 respectively) registered during the cooling of Al-5Si3Cu alloy from the liquid phases, in tec-tip standard cup.

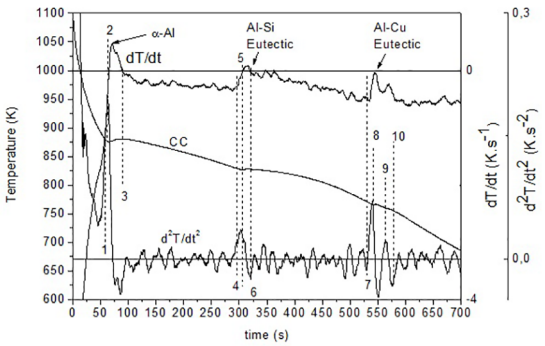

Figure 2. The cooling curve, the first and second derivative curves (dT/dt and d^2T/dt^2 respectively) of Al-5Si3Cu alloy solidified in tec-tip standard cup.

A summary of metallurgical events corresponding to the solidification sequence, identified directly from the cooling curve (figure 2) showed in table 2.

It is evident in figure 2 that the cooling rate widely varies during the solidification of alloy. In general, the cooling rate is calculate from the slope of cooling curve before *liquidus* temperature ($T^{\alpha\text{-}Al}_N$). Otherwise, the cooling rate in the mushy zone is compute by dividing the total solidification temperature to the total solidification time[8,9,12].

In the present work, the cooling rate in the liquid phase region computed by $\Delta T_L(K)/\Delta t_L(s)$ equation for the alloy solidified in tec-tip standard cup was 3.7 K/s. Similarly, the cooling rate in semi-solid phase verified by $(T^{\alpha\text{-}Al}_N - T_{solidus})/(t_S - t_L)$ equation was 0.24 K/s, where the solidification range is defined as the difference in temperatures between the first ($T^{\alpha\text{-}Al}_N$) and the last liquid to solidify ($T_{solidus}$), and the total solidification time (t_s-t_L) is the range between the start and the end of solidification.

The *liquidus* and *solidus* temperatures (point1 and point10 in table 2), as well as in the eutectic reactions temperatures registered in cooling curve (figure 2) are different from Al-Si-Cu ternary phase diagram[6], mainly due to the cooling rate used. In table 2, the silicon eutectic reaction (point 4) is 20 K and the copper eutectic reaction (point 7) is 54 K lower than the recorded in equilibrium diagrams[2]. Narayanan et al.[6] and Taylor[13] found similar results for the same solidified alloy with moderate cooling rate.

Figure 3 shows BSE (backscattered electrons) images of the alloys 319.2 sample solidified in tec-tip standard cup. It is interesting to observe in figure 3.a the presence of the needles (light gray), different silicon structures typical of unmodified Al–Si foundry alloys (dark gray), as well as, eutectic strutures Al + Al_2Cu (light) present mostly along the needles.

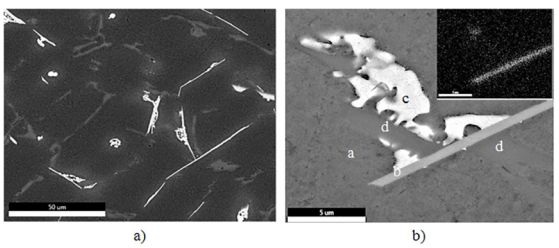

Figure 3. a) the BSE-SEM image as-casting microstructure of Al-5Si3Cu alloy ingot solidified in tec-tip standard cup at cooling rates of 0.24 K/s of in mushy zone. Figure b) detail of alloy microstructure. The inset corresponds to the iron EDS map. The phase related to the amount of iron over the (c) phase was not identified.

Figure 3.b shows details the alloy microstructure, i.e., α–Al dendrites (a), needle of the β-Fe_5AlSi phase (b), Cu-rich eutectic structures (c) and, silicon structures (d). Note that silicon structures do not present sufficient contrast in

Table 2. The solidification characteristic parameters of phase evolution for Al-5Si3Cu alloy solidified in tec-tip standard cup by thermal analysis.

Point	Symbol	Description	T (K)
1	$T^{\alpha\text{-}Al}_N$	α-Al dendrite nucleation (liquidus temperature)	880
2	$T^{\alpha\text{-}Al}_{min}$	α-Al minimum phase	875
3	$T^{\alpha\text{-}Al}_G$	α-Al growth phase	879
4	$T^{Al\text{-}Si}_N$	Al-Si primary eutectic nucleation	830
5	$T^{Al\text{-}Si}_{min}$	Al-Si primary eutectic minimum	827
6	$T^{Al\text{-}Si}_G$	Al-Si primary eutectic growth	826
7	$T^{Al_2Cu}_N$	Al_2Cu secondary eutectic nucleation	767
8	$T^{Al_2Cu}_{min}$	Al_2Cu secondary eutectic minimum	765
9	$T^{Al_2Cu}_G$	Al_2Cu secondary eutectic growth	767
10	$T_{solidus}$	End of solidification	757

matrix relation in BSE images. There is a significant fraction of growing coupled to needles β-Al_5FeSi and the silicon structures in the interdendritic regions. The insert in figure 3.b show the iron EDS map of the figure 3.b. The microstructural composition of the sample in figure 3.b. was confirmed by EDS microanalysis, as show in table 3. The phase related to the amount of iron over the Cu-rich eutectic structures (c) was not identified. It is necessary to emphasize that the analyzes by ESD are qualitative because they depend on the chemical composition of the analyzed material.

Dinnis[10,11] and Taylor et al.[13], under analogous conditions used in this work, verified that the iron-containing phases crystallizes only in Chinese scripts morphology, when the cooling rate in semisolid phase equal to 0.2 K/s. However, figure 3 reveals only the existence of needles of the β-Al_5FeSi phase (see figure 3) in the microstructure of the alloy solidified with a cooling rate of 0.24 K/s in the mushy zone.

Another interesting fact is that the cooling curve in figure 2 does not register the typical 319.0 alloy plateau, related to the formation of needles of the β-Al_5FeSi phase between 3-4 points as described in the literature[6,10,11,13]. This suggests that the formation of needles of the β-Fe_5AlSi phase occurs just before the eutectic Al-Si phase. Narayanan[6] and Timelli[8] show that the reaction plateau associated to the formation of the β-iron phase do not appear in the cooling curve when it merges with the eutectic Al-Si peaks and valleys. The same authors show that the area fraction of the primary β-phase needles greatly depends on the time interval between the β-phase start temperature and the silicon eutectic temperature[6,8].

3.2. Solidification in high cooling rates

In figure 4, it is possible to observe the cooling curves (temperature (K) / time (s)), registered during the cooling of Al-5Si3Cu alloy from the liquid phases, solidified in the metallic six-step cylindrical mold. The lines $T^{\alpha\text{-}Al}{}_N$ and $T_{solidus}$ in figure 4 refer to the *liquidus* and *solidus* temperatures recorded by the thermal analysis system during the experiments realized by tec-tip standard cup (see table 2). We used these

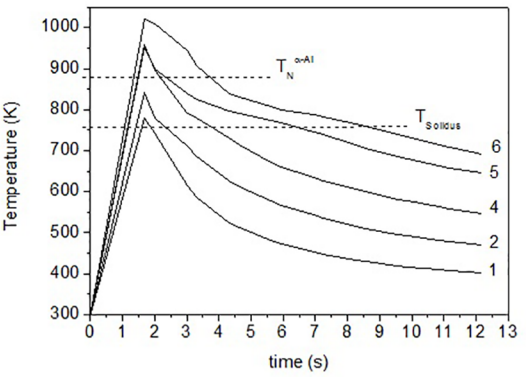

Figure 4. Cooling curves of Al-5Si3Cu alloy solidified in six-stepped cylindrical steel mold recorded by the thermocouples 1,2 4, 5 and 6. Where Tα-AlN is equal to 880 K and $T_{solidus}$ to 757 K.

and other data from table 2 to compare the evolution of the cooling curves and the alloy microstructure solidified in a six-stepped cylindrical steel mold.

Table 4 shows the cooling rates in the semi-solid phase estimated by steps in metallic mould. The cooling rate for the steps 4, 5 and 6 are obtained directly from the cooling curves. Due to the high rates of heat extraction involved in steps 1, 2 and 3, the cooling rate are calculated by the Chvorinov's rule[1].

In the data analysis of figure 4, we observed that the total solidification time decreases for all diameter of the stepped-metallic mold, as expected. Due to the cooling rates involved in the experiments only is possible to identify the ($T^{\alpha\text{-}Al}{}_N$) α-Al dendrite nucleation temperature for steps 6, 5 and 4. It was not possible to identify the ($T^{\alpha\text{-}Al}{}_G$) α-Al growth phase temperature, the supercooling and the recalecence in the curves of the figure 4. However it is possible to identify the temperatures of the Al-Si primary eutectic nucleation ($T^{Al\text{-}Si}{}_N$) and the Al_2Cu secondary eutectic nucleation ($T^{Al_2Cu}{}_N$) for all six steps. Note in figure 4 that ($T^{\alpha\text{-}Al}{}_N$) the α-Al dendrite nucleation temperature for steps 6, 5 and 4 increase according as the cooling rate increases. On the other hand, we find that the $T^{Al\text{-}Si}{}_N$ (Al-Si primary eutectic nucleation temperture) decreases according as the cooling rate increases, for all steps.

Table 3. EDS analysis of figure 3.b and the suggested phase (atomic %).

Point	Al	Si	Cu	Fe	Mn	total	Suggested phases
(a)	98.44	1.28	0.24	0.03	0.01	100	α-Al dendrite
(b)	80.42	10.65	0,94	6.32	1.66	100	β-Al_5FeSi
(c)	74.24	21.33	-	-	1.43	100	Silicon eutectic
(d)	71.98	-	28.02	-	-	100	Eutectic Al-Cu

Table 4. Cooling rates in semi-solid region estimated by cooling curve, mean linear length (MLL) of dendritic and Vickers microhardness (HV) of Al-5Si3Cu solidified in six-stepped cylindrical steel mold. (*) cooling rates calculate by Chvorinov's rule[1].

Step	1	2	3	4	5	6
Cooling rate (K/s)	815*	137*	75*	42	32	24
Dendritic MLL (μm) Standard deviation	10.06 ± 5.60	16.98 ± 3,11	20,01 ± 2,01	26,14 ± 5,30	28,13 ± 1,83	30,91 ± 2,82
Vickers microhardness (HV)	97.4	96.2	91.0	88.1	93.0	94.7

The mean linear length of dendritic showed in table 4 increases according as the cooling rate decreases. According to the literature[6-8,11,16], this behavior is due to the increase of the supercooling resulting from the increase of the cooling rate. The higher the cooling rate the greater the α-Al dendrite nucleation temperature ($T^{\alpha\text{-}Al}_{N}$), the supercooling and the lower the recalescence, so the α-Al growth phase temperature ($T^{\alpha\text{-}Al}_{G}$) decreases and thus, the many nucleus formed have the energy to grow, increasing the number of grain.

Solidified samples in stepped-metal mold showed higher Vickers microhardness than the 67.2 HV found in the sample solidified in tec-tip standard cup. However, table 4 shows that the microhardness decreases from steps 6 to 4 and then increases again from steps 5 to 6. An explanation of this behavior is in the microstructure of the samples shown in figure 5.

In the step 1 sample in figure 5 (a and b), note polygonal particles of the eutectic Al-Si *(EDS map*) together as not-well-

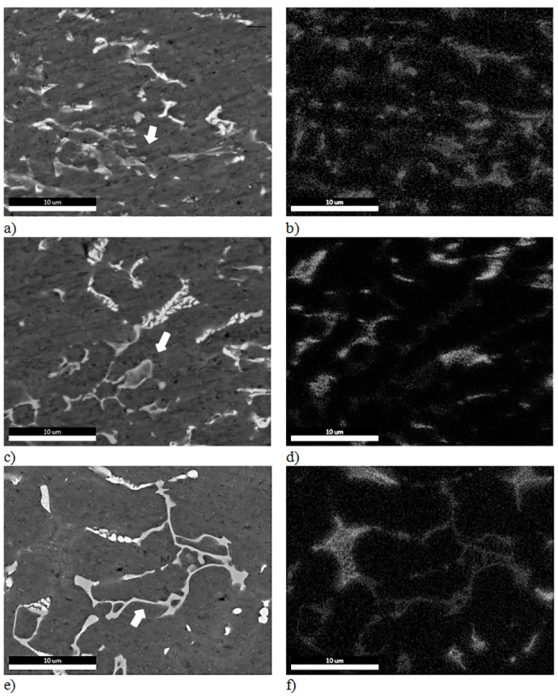

Figure 5. BSE images of the step 1 (a), step 3 (c) and step 6 (e). Silicon ESD map of the the step 1 (b), step 3 (d) and step 6 (f) of ingots of Al-5Si3Cu solidified in the six-stepped cylindrical steel mold. The arrows point to the α_c-$Al_{15}(Fe,Mn)_3Si_2$ phase.

developed α_c-$Al_{15}(Fe,Mn)_3Si_2$ (*arrows point)* and small and elongated plates of Al_2Cu (light). In the step 3 sample figure 5 (c and d) we notice a infrequent and better developed Chinese scripts α_c-$Al_{15}(Fe,Mn)_3Si_2$ phase (*arrows point)*, the Al-Si eutectic in the grain boundary *(EDS map*), and the eutectic lamellae Al-Al_2Cu . On the other hand, the microstructure of step 6 sample in figure 5 (e and f) shows the well-developed Chinese scripts morphology α_c-$Al_{15}(Fe,Mn)_3Si_2$ phase (*arrows point)* and Al-Si eutectic phase in the grain boundary *(EDS map*), and formations of the secondary lamellae Al-Al_2Cu. No needles β-phase were found in the samples solidified in the metal mold. Therefore, the decrease of the microhardness observed for the samples of steps 1 to 4, and the subsequent increase of hardness to step 6 (see table 3) is attributed to at least two factors: the gradual increase of the grain size from step 4 and the presence of the well-defined α_c-$Al_5(Fe,Mn)_3Si_2$ phase[4,6,7,13].

4. Conclusion

For the Al-Si5Cu3 alloy the results obtained in this work confirm that cooling rates influence the nucleation and growth of α_c-$Al_{15}(Fe,Mn)_3Si_2$ and β- Al_5FeSi phases.

The micrography of the Al-Si5Cu3 alloy reveals the presence of needle-like β-Al_5FeSi phase and the absence of α_c-$Al_{15}(Fe,Mn)_3Si_2$ in the microstructure of the alloy solidified in a low cooling rate (3.7 K/s in the liquid zone and 0.24 K/s in the mushy zone). Absence of the the plateau of the β-Al_5FeSi phase in the correspondent cooling curve indicates that the formation of needles of the β-Fe5AlSi phase take place just before the eutectic Al-Si phase.

The solidification experiment in the six-stepped metallic mold, indicated that the α-Al dendrite nucleation temperature ($T^{\alpha\text{-}Al}_{N}$) increase according as the cooling rate increases and, the $T^{Al\text{-}Si}_{N}$ and $T^{Al_2Cu}_{N}$ decrease according as the cooling rate increases. Experiments with the stepped mold show that the difference between the $T^{Al\text{-}Si}_{N}$ and $T^{Al_2Cu}_{N}$ temperatures decreases according as the cooling rate increases for the studied alloys.

β-phase needles were not found in the solidification samples in the metal stepped mold, different from what occurred in the tec-tip standard cup. Only when the cooling rate in the mushy zone was less than 75 K/s, it was possible to observe the well-developed script Chinese α-$Al_{15}(Fe,Mn)_3Si_2$ phase. This proves that the detrimental β-phase formation can be eliminated in Al-Si5Cu3 alloys containing 1.0% Fe, 0.5% Mn, with a superheating of 800 K, and cooling rates higher than 24 K/s.

5. Acknowledgments

The authors would like to thank the BPA program of Pontifical Catholic University of Rio Grande do Sul (PUCRS), the National Council for Scientific and Technological Development of Brazil (CNPq) and the Foundation for Research Support of Rio Grande do Sul (FAPERGS) for scholarships and for supporting their research.

6. References

1. Campbell J. *Complete Casting Handbook*. 2nd ed. Oxford: Elsevier; 2015. 1054 p.

2. Kaufman JG, Rooy EL. *Aluminum Alloy Castings: Properties, Processes, and Applications*. Materials Park: ASM International; 2004.

3. Yi JZ, Gao YX, Lee PD, Lindley TC. Effect of Fe-content on fatigue crack initiation and propagation in a cast aluminum–silicon alloy (A356–T6). *Materials Science and Engineering: A*. 2004;386(1-2):396-407.

4. Seifeddine S, Johansson S, Svensson IL. The influence of cooling rate and manganese content on the β-Al5FeSi phase formation and mechanical properties of Al–Si-based alloys. *Materials Science and Engineering: A*. 2008;490(1-2):385-390.

5. Puncreobutr C, Lee PD, Kareh KM, Connolley T, Fife TL, Phillion AB. Influence of Fe-rich intermetallic on solidification defects in Al–Si–Cu alloys. *Acta Materialia*. 2014;68:42-51.

6. Narayanan LA, Samuel FH, Gruzleski JE. Crystallization behavior of iron-containing intermetallic compounds in 319 aluminum alloy. *Metallurgical and Materials Transactions A*. 1994;25(8):1761-1773.

7. Yang W, Gao F, Ji S. Formation and sedimentation of Fe-rich intermetallics in Al−Si−Cu−Fe alloy. *Transactions of Nonferrous Metals Society of China*. 2015;25(5):1704-1714.

8. Timelli G, Capuzzi S, Fabrizi A. Precipitation of primary Fe-rich compounds in secondary $AlSi_9Cu_3(Fe)$ alloys. *Journal of Thermal Analysis and Calorimetry*. 2016;123(1):249-262.

9. Emadi D, Whiting LV, Nafisi S, Ghomashchi R. Applications of thermal analysis in quality control of solidification processes. *Journal of Thermal Analysis and Calorimetry*. 2005;81(1):235-242.

10. Dinnis CM, Taylor JA, Dahle AK. Iron-related porosity in Al-Si-(Cu) foundry alloys. *Materials Science and Engineering: A*. 2006;425(1-2):286-296.

11. Dinnis CM, Taylor JA, Dahle AK. As-cast morphology of iron-intermetallics in Al-Si foundry alloys. *Scripta Materialia*. 2005;53(8):955-958.

12. Farahany S, Ourdjini A, Idris MH, Shabestari SG. Computer-aided cooling curve thermal analysis of near eutectic Al–Si–Cu–Fe alloy. *Journal of Thermal Analysis and Calorimetry*. 2013;114(2):705-717.

13. Taylor JA. Iron-Containing Intermetallic Phases in Al-Si Based Casting Alloys. *Procedia Materials Science*. 2012;1:19-33.

14. ASTM International. *ASTM E112-96 (2004) - Standard Test Methods for Determining Average Grain Size*. West Conshohocken: ASTM International; 2004.

15. ASTM International. *ASTM E384-16 - Standard Test Method for Microindentation Hardness of Materials*. West Conshohocken: ASTM International; 2016.

16. Uzon O, Karaaslan T, Keskin M. Production and Structure of Rapidly Solidified Al-Si Alloys. *Turkish Journal of Physics*. 2001;25:455-466.